

Article

Application of a Novel Bifunctionalized Magnetic Biochar to Remove Cr(VI) from Wastewater: Performance and Mechanism

Xiangfen Cui¹, Juan Wang¹, Qun Zhao¹, Chen Li¹, Jianhong Huang¹, Xuwei Hu¹, Jie Li^{1,*} and Mantao Li^{2,*}

¹ Faculty of Environmental Science and Engineering, Kunming University of Science and Technology, 727 South Jingming Road, Chenggong District, Kunming 650500, China; cui1987rainny@163.com (X.C.); wjuan18387436920@163.com (J.W.); lcshirley@163.com (C.L.); huangjianhong78@163.com (J.H.); huxuewei@kust.edu.cn (X.H.)

² Faculty of Land Resource Engineering, Kunming University of Science and Technology, 68 Wenchang Road, Wuhua District, Kunming 650093, China

* Correspondence: lj478425753@163.com (J.L.); limantao_kmust@sina.com (M.L.); Tel./Fax: +86-871-6592-0521 (J.L.)

Abstract: Biochar adsorption has emerged as a favorable and environmentally friendly approach for removing metals such as chromium (Cr) from wastewater. However, the use of pristine biochar (PBC) is limited due to its finite adsorptive capacity, selectivity, and potential for secondary pollution. In this study, a novel bifunctionalized magnetic biochar (BMBC) was fabricated by incorporating cystamine as a ligand and glutaraldehyde as a crosslinker into alkali-treated magnetic biochar (MBC). This chemical modification introduced numerous amino groups and disulfide bonds onto the surfaces of BMBC. The biochar adsorbents' surface morphologies, crystal structures, and texture properties were characterized using SEM, XRD, and N₂ adsorption-desorption techniques. The specific surface area was determined using the BET method. Furthermore, the surface functional groups and elemental compositions before and after adsorption were analyzed using FTIR and XPS, respectively. The results demonstrated higher Cr(VI) removal efficacy of BMBC (100%) than MBC (72.37%) and PBC (61.42%). Optimal conditions for Cr(VI) removal were observed at a solution pH of 2, a temperature of 50 °C, a reaction time of around 1440 min, and an initial adsorbate concentration of 300 mg/L. The sorption process followed a chemical mechanism and was controlled by monolayer adsorption, with a maximum adsorption capacity of 66.10 mg/g at 50 °C and a pH of 2, as indicated by the larger fitting values of the pseudo-second-order and Langmuir models. The positive ΔH° and ΔS° values and negative ΔG° values suggested a spontaneous and endothermic Cr(VI) adsorption process with high randomness at the solid/liquid interface. The removal of Cr(VI) was attributed to the reduction of Cr(VI) into Cr(III) facilitated by the introduced amino acids, sulfur, and Fe(II), electrostatic interaction between Cr(VI) in the solution and positive charges on the adsorbent surface, and complexation with functional groups. The presence of co-existing cations such as Cu(II), Cd(II), Mn(II), and K(I) had little effect on Cr(VI) removal efficiency. At the same time, the co-existence of anions of Cl⁻, NO₃⁻, SO₄²⁻, and HPO₄²⁻ resulted in a 7.58% decrease in the Cr(VI) removal rate. After five consecutive adsorption/desorption cycles, BMBC maintained a high Cr(VI) removal rate of 61.12%. Overall, this novel BMBC derived from rice straw shows great promise as a biosorbent for treating Cr(VI) in wastewater.

Keywords: magnetic biochar; bifunctionalization; chemical modification; hexavalent chromium; adsorption



Citation: Cui, X.; Wang, J.; Zhao, Q.; Li, C.; Huang, J.; Hu, X.; Li, J.; Li, M. Application of a Novel Bifunctionalized Magnetic Biochar to Remove Cr(VI) from Wastewater: Performance and Mechanism. *Separations* **2023**, *10*, 358. <https://doi.org/10.3390/separations10060358>

Academic Editors: Andrey E. Krauklis and Ivar Zekker

Received: 22 May 2023

Revised: 4 June 2023

Accepted: 11 June 2023

Published: 15 June 2023



Copyright: © 2023 by the authors. Licensee MDPI, Basel, Switzerland. This article is an open access article distributed under the terms and conditions of the Creative Commons Attribution (CC BY) license (<https://creativecommons.org/licenses/by/4.0/>).

1. Introduction

Aquatic heavy metals control has gained significant attention worldwide due to the extreme toxicity of these metals to living organisms, their high potential for bioaccumulation and biomagnification, as well as their extensive use in various industries [1,2]. Chromium

hexavalent (Cr(VI)) is highly soluble and mobile in aquatic environments, and its compounds are known to be carcinogenic to humans [3]. Cr(VI)-containing compounds can oxidize to form free radicals and can be reduced to less oxidative and toxic states, such as Cr(III) [4]. Therefore, developing efficient strategies and technologies for removing Cr(VI) from aquatic environments is crucial to safeguarding against the ecological and health damage caused by Cr(VI) exposure.

Adsorption is widely regarded as a favorable method for removing Cr(VI) from wastewater [5,6] compared to other approaches such as electrocoagulation [7], ion exchange [8], and membrane separation [9]. Adsorption offers easy operation, high efficiency, and cost-effectiveness [10]. Herein, it is crucial to design and fabricate economical, efficient, and environmentally friendly adsorbents [11]. Commonly used adsorbents such as biochar [12,13], activated carbon [14,15], and chitosan [16,17], as well as advanced adsorbents such as metal-organic framework [18], have been developed as adsorbents for adsorbing contaminants from wastewater. Among them, biochar, an empirically proven carbonaceous material produced through pyrolysis of carbon-rich biomass under anaerobic conditions [19,20], has found extensive application in the environmental and energy fields. Its widespread use can be attributed to its abundant availability from diverse biomass sources, high removal efficiency due to its porous microstructure and surface functional groups, as well as its environmentally benign nature without causing secondary pollution [2,14,21].

Crop straw has been increasingly used in prior studies as a feedstock for producing biochar for treating wastewater [22]. Rice, being the most widely consumed cereal grain, has served as a staple food for over half of the global population. In 2021, global rice production exceeded 780 million tons, with China and neighboring countries such as India and Bangladesh representing nearly 60% of the total production [23]. After the rice grains are harvested, approximately half of the rice plant's non-edible biomass remains as rice straw [24]. As a significant crop residue in China, rice straw reached over 200 million tons in 2021, which poses environmental challenges such as greenhouse gas emissions when left underutilized or burned [25,26]. In addition, rice straw has a fixed carbon content exceeding 16% and moisture content lower than 5%, making it suitable for pyrolysis to produce biochar [22].

However, the use of pristine biochar (PBC) is limited due to its low porosity, surface functionality, small specific surface area (SSA), finite sorption capacity in high-concentration solution systems, and lack of selectivity in co-existing systems [12,21,22,27]. Surface modification has emerged as a promising approach to enhancing adsorption capacity and specificity by introducing sites in increased SSA and strengthening the adsorption affinity of specific surface functional groups [28,29]. Amino groups have been widely investigated for their ability to complex with metals, rendering the widespread application of N-containing organic groups such as amines, aromatic amines, and amides in the removal of Cr(VI) from wastewater [30–33]. In acidic solutions, surface amino groups are protonated to form positively charged sites ($-\text{NH}_3^+$) that subsequently bind with anionic Cr(VI) through electrostatic interaction [30]. As electron donor groups, surface amine groups facilitate the reduction of Cr(VI) to Cr(III), which is less toxic [34,35]. However, Cr(III) may be released into the solution with an increase in contact time [29], highlighting the necessity for simultaneous reduction-coupled adsorption processes for Cr(VI) and Cr(III). Based on the hard–soft acid–base theory, Cr(III) is a softer base that tends to be captured by softer acids, such as sulfur [17]. Herein, a promising approach to enhance the adsorption capacity and ensure feasible reduction-coupled adsorption is the modification of biochar with cystamine ($\text{NH}_2-(\text{CH}_2)_2-\text{S}-\text{S}-(\text{CH}_2)_2-\text{NH}_2$), which contains abundant amino groups and disulfide bonds [28].

Another significant issue is the separation of polluted adsorbents from aquatic systems after adsorption, as this may lead to secondary environmental pollution [6,30,36]. Magnetic biochar (MBC) has been observed to possess outstanding magnetism, enabling the separation of metal-contained adsorbents from wastewater [36,37]. In this study, a

novel bifunctionalized magnetic biochar composite (BMBC) was developed for removing Cr(VI) from wastewater by incorporating cystamine as a ligand and glutaraldehyde as a crosslinker into alkali-treated MBC, and its properties, adsorption performance, and mechanisms of Cr(VI) removal were investigated in detail. For comparison, BMC was obtained from the co-pyrolysis of PBC and a mixed solution of Fe(III)/Fe(II), while the pyrolysis of dried rice straw powder prepared PBC. It was hypothesized that BMBC would exhibit superior Cr(VI) adsorption due to increased binding sites on its surface, stronger complexation, and electrostatic interaction between Cr(VI) and surface functional groups. The specific goals of this study were: (1) to examine the determining properties of BMBC for Cr(VI) adsorption; (2) to compare the adsorption performance of BMBC with that of BMC and PBC under varying solution pH, reaction time, temperature, initial adsorbate concentration, and the presence of co-existing anions and cations; and (3) to elucidate the mechanisms underlying Cr(VI) adsorption.

2. Materials and Methods

2.1. Materials and Chemicals

Rice straw, obtained from farmland in Kunming, southwest China, was used as the feedstock biomass. Ferric chloride hexahydrate ($\text{FeCl}_3 \cdot 6\text{H}_2\text{O}$), ferrous sulfate ($\text{FeSO}_4 \cdot 7\text{H}_2\text{O}$), glutaraldehyde ($\text{C}_5\text{H}_8\text{O}_2$), cystamine dihydrochloride ($\text{C}_4\text{H}_{12}\text{N}_2\text{S}_2 \cdot 2\text{HCl}$) and 1,5-diphenyl carbazide ($\text{C}_{13}\text{H}_{14}\text{N}_4\text{O}$) were purchased from Aladdin, Shanghai, China. Potassium dichromate ($\text{K}_2\text{C}_2\text{O}_7$), nitric acid (HNO_3), hydrochloric acid (HCl), sodium hydroxide (NaOH), cupric chloride ($\text{CuCl}_2 \cdot 2\text{H}_2\text{O}$), cadmium chloride ($\text{CdCl}_2 \cdot 2.5\text{H}_2\text{O}$), manganese chloride ($\text{MnCl}_2 \cdot 4\text{H}_2\text{O}$), potassium chloride (KCl), sodium nitrate (NaNO_3), sodium sulfate (Na_2SO_4), sodium phosphate (Na_2HPO_4), and ethanol ($\text{C}_2\text{H}_6\text{O}$) were obtained from Shanghai Macklin Biochemical Co., Ltd., China, as residual reagents. All chemicals used for this work were of analytical grade. The experimental solutions were prepared using deionized water (18.2 M Ω).

2.2. Fabrication of Biochar Adsorbents

Three biochar adsorbents, BMBC, MBC, and PBC, were prepared for subsequent experiments. PBC was fabricated by heating 20 g of feedstock in a box resistance furnace at 600 °C for 3 h and sieving the resulting materials through a 200-mesh sieve. MBC was prepared via pyrolysis as follows: 15 g of raw rice straw powder was dispersed in a mixture of 3 g $\text{FeCl}_3 \cdot 6\text{H}_2\text{O}$ and 3 g $\text{FeSO}_4 \cdot 7\text{H}_2\text{O}$ in 300 mL deionized water, shaken well at room temperature, then subjected to ultrasonic treatment for 2 h, immersed for 24 h, dried at 70 °C, and then pyrolyzed at 600 °C for 3 h in a box resistance furnace. The resulting MBC material was sieved through a 200-mesh sieve. Following the method described by Zhang et al. (2013), BMBC was obtained by chemically modifying alkali-treated BMC using cystamine and glutaraldehyde as ligands and crosslinkers, respectively. Initially, 10 g of MBC was mixed with 100 mL of 3 mol/L NaOH (pH = 13.78) for alkali treatment. After 2 h of reaction at 60 °C, the alkali-treated MBC particles were washed with ethanol and deionized water until the pH value was nearly neutral. The particles were then oven-dried at 70 °C. Subsequently, a 50 mL aqueous solution of glutaraldehyde (2%, v/v) was added to 7 g of the alkali-treated MBC, and the mixture was stirred for 4 h at room temperature. Then, 1.5 g of cystamine dihydrochloride was gradually added, and the stirring was continued for 12 h. Finally, the solid BMBC was separated using an external magnet and washed with ethanol and deionized water until the pH value was constant.

2.3. Characterization of Biochar Adsorbents

The surface morphologies of biochar adsorbents were examined using a scanning electron microscope (SEM, Nova NanoSEM 450, FEI, Hillsborough, OR, USA). Their texture properties were evaluated by conducting N_2 adsorption-desorption measurements at 300 °C for 8 h. The SSA was determined by the Brunauer–Emmett–Teller (BET) method, and the porosities were analyzed using an automatic analyzer (Autosorb IQ3, Quantachrome,

Boynton Beach, FL, USA). The pore size distribution and pore volume were determined using the Horvath–Kawazo and Barrett–Joyner–Halenda methods, respectively [30]. The crystal structures of the adsorbents were characterized using X-ray diffraction (XRD, UltimaIV, Neo Confucianism, Tokyo, Japan) in the range from 10° to 80° at a speed of 10° per minute. The surface functional groups were analyzed using Fourier transform infrared spectroscopy (FTIR, Nicolet iS5, Thermo Electron, Waltham, MA, USA) with 32 scans over a 4000 to 400 cm⁻¹ wavelength range and a resolution of 4 cm⁻¹. The elemental composition of the adsorbents before and after adsorption was analyzed using X-ray photoelectron spectroscopy (XPS, K-Alpha 1063, Thermo Fisher, Waltham, MA, USA), and the original binding energy was corrected based on the C1s peak at 1486.6 eV. The zeta potential of the suspension was measured using a Zetasizer nano series Nano ZS 90 instrument (Malvern Panaco, Malvern, UK). The magnetic properties were determined using a vibrating sample magnetometer (VSM, 7404, Lakeshore, Columbus, OH, USA) with a magnetic field range of ±2.

2.4. Batch Sorption

2.4.1. Preparation of Cr(VI) Aqueous Suspension

The Cr(VI) solution for the subsequent experiments was prepared by dissolving 2.8290 g of potassium dichromate (K₂C₂O₇) in 1000 mL of deionized water, resulting in a Cr(VI) stock solution with a concentration of 1000 mg/mL [34,38]. K₂C₂O₇ was first heated at 100 °C for 2 h and cooled to room temperature to prepare the stock solution. Subsequently, 2.8290 g of K₂C₂O₇ was diluted with deionized water and transferred into a 1000 mL volumetric flask to reach the desired volume. The solution was thoroughly mixed and stored in a cool, dark place for later use. The concentration of Cr(VI) in the solution was determined using the 1,5-diphenylcarbazide colorimetric method, which involved measuring the absorbance of the solution at the optimal wavelength of 540 nm using a UV–visible spectrophotometer. The concentration of Cr(VI) was found to be linearly correlated with the intensity of the absorbance signals ($R^2 > 0.999$).

2.4.2. Experiments for Cr(VI) Adsorption

All static adsorption experiments were performed in a 200 mL conical flask by adding 20 mg adsorbents to a 10 mL stock solution. The conical flasks were agitated at 150 rpm in a thermostatic shaking incubator until equilibrium was reached. After separating the solid mixture from the liquid using an external magnet, the residues were extracted and filtered to determine the concentration of Cr(VI). The effects of reaction time (5–2160 min), initial concentration of Cr(VI) (10–500 mg/L), solution pH (2–8), competitive cations (Cu(II), Mn(II), Cd(II), K(I)), and anions (Cl⁻, NO₃⁻, SO₄²⁻, HPO₄²⁻) on Cr(VI) adsorption were investigated. Following prior experiments [30,34], the capacity (Q_e) and efficiency (η , %) of removal were quantified based on the solution concentrations of Cr(VI) before and after adsorption using Equations (1) and (2).

$$Q_e = \frac{(C_0 - C_e)V}{m} \quad (1)$$

$$\eta\% = \frac{C_0 - C_e}{C_0} \times 100\% \quad (2)$$

where C_0 represents the initial concentration of Cr(VI) (mg/L) before adsorption, and C_e denotes the final concentration of Cr(VI) (mg/L) after adsorption. V is the solution volume (L), and m is the mass (g) of the adsorbates.

2.4.3. Adsorption Kinetics

Time-dependent experiments were carried out to investigate the adsorptive rate of Cr(VI) onto biochar adsorbents. A total of 20 mg of biochar adsorbents was added to 10 mL of Cr(VI) solution at 50 mg/L with different contact times ranging from 5 to 2160 min.

The pH of the solution was adjusted to 2 using 1 mol/L HNO₃ and 1 mol/L NaOH. The kinetic data obtained was fitted using the pseudo–first-order model (Equation (3)), pseudo–second-order model (Equation (4)), and intraparticle diffusion model (Equation (5)) to quantitatively evaluate the capture of Cr(VI) on the different biochar adsorbents. The optimal kinetic model was selected according to the largest coefficient of determination (*R*²).

$$\ln(Q_e - Q_t) = \ln Q_e - K_1 t \tag{3}$$

$$\frac{t}{Q_t} = \frac{1}{K_2 Q_e^2} + \frac{1}{Q_e} t \tag{4}$$

$$Q_t = K_p t^{\frac{1}{2}} + C \tag{5}$$

where *Q_e* and *Q_t* represent the capacity (mg/g) to adsorb Cr(VI) at equilibrium and at time *t*, respectively. *K*₁ (1/min), *K*₂ (g/mg/min), and *K_p* (g/mg/min^{1/2}) are the rate constants for pseudo–first-order, pseudo–second-order, and intraparticle diffusion models, respectively. The constant *C* is the intercept of the intraparticle diffusion model, which reflects the thickness of the boundary layer.

2.4.4. Equilibrium Isotherm

The Langmuir and Freundlich models are commonly used to describe sorption behavior based on different assumptions [15,39]. The Langmuir model assumes that the adsorbents do not interact with finite active sites within a monolayer of homogenous chemisorption. On the other hand, the Freundlich model considers the heterogeneous energetic distribution of active sites and accounts for the multilayer uptake of adsorbates. In this study, isotherm adsorption was investigated by mixing 20 mg of adsorbents with Cr(VI) solution at varying concentrations (10 mg/L, 25 mg/L, 50 mg/L, 100 mg/L, 200 mg/L, 300 mg/L, 400 mg/L, and 500 mg/L) at temperatures of 30 °C, 40 °C and 50 °C. After the adsorption process, the concentration of Cr(VI) in the solution was determined by shaking the mixture for 24 h. The obtained isotherm data were fitted using the Langmuir (Equations (6) and (7)) and Freundlich (Equation (8)) equations.

$$\frac{C_e}{Q_e} = \frac{1}{Q_{\max} K_L} + \frac{1}{Q_{\max}} C_e \tag{6}$$

$$R_L = \frac{1}{(1 + K_L C_0)} \tag{7}$$

$$Q_e = K_F C_e^{\frac{1}{n}} \tag{8}$$

where *Q_e* and *Q_{max}* represent equilibrium and the maximum quantity (mg/g) of Cr(VI) adsorbed onto adsorbents, respectively. *C_e* and *C₀* denote the equilibrium and initial concentration (mg/L) of Cr(VI), respectively. The parameter *K_L* (L/mg) is an energy constant, and *n* reflects the adsorption intensity. *R_L* is a separation factor estimating the feasibility of adsorption, which is favorable when *R_L* ranges from 0 to 1 [15,40]. *K_F* (mg^{1–*n*} L^{*n*}/g) is a coefficient related to the adsorption capacity.

2.4.5. Adsorption Thermodynamics

The spontaneity, extent of the driving force, and energy involved in the adsorption of Cr(VI) onto adsorbents were further investigated by analyzing the changes of Gibbs free energy (ΔG° , KJ/mol), entropy (ΔS° , J/(K·mol)), and enthalpy (ΔH° , KJ/mol) according to Equations (9) and (10) [15,40].

$$\Delta G^\circ = -RT \times \ln K_a \tag{9}$$

$$\ln K_a = \frac{\Delta S^\circ}{R} - \frac{\Delta H^\circ}{RT} \tag{10}$$

where K_a represents the constant related to thermodynamic equilibrium. R is a general gas constant set at 8.314 J/(K·mol), and T is the absolute temperature. A positive value of ΔH° indicates an endothermic reaction during the adsorption process, while a negative value of ΔH° indicates that the adsorption process occurs spontaneously and is feasible.

2.4.6. Stability and Re-Usability Assessment

A total of five consecutive adsorption/desorption cycles were performed to assess the stability and re-usability of adsorbents. In each cycle, the adsorbents were subjected to desorption by washing with 0.2 mol/L of NaOH after the adsorption step. The washed adsorbents were then filtered, washed with deionized water, and dried before being reused in the subsequent cycle. The removal rates of the adsorbents were determined according to Equation (2).

3. Results and Discussions

3.1. Biochar Characterization

As shown in Figure 1, the biochar adsorbents exhibit distinct surface morphologies. PBC displays smooth surfaces with apparent pores but lacks fine particles and polymers within the pores (Figure 1A,a). On the other hand, the inner surface of BMC pores appears rough and contains noticeable aggregated particles (Figure 1B,b). Notably, BMBC exhibits abundant particulate polymers closely adhering to the pore surface (Figure 1C,c). The rougher inner surface of BMC pores compared to PBC may be attributed to loaded Fe_3O_4 particles. In contrast, the presence of particulate polymers on BMBC could potentially enhance its capacity for adsorbing Cr(VI).

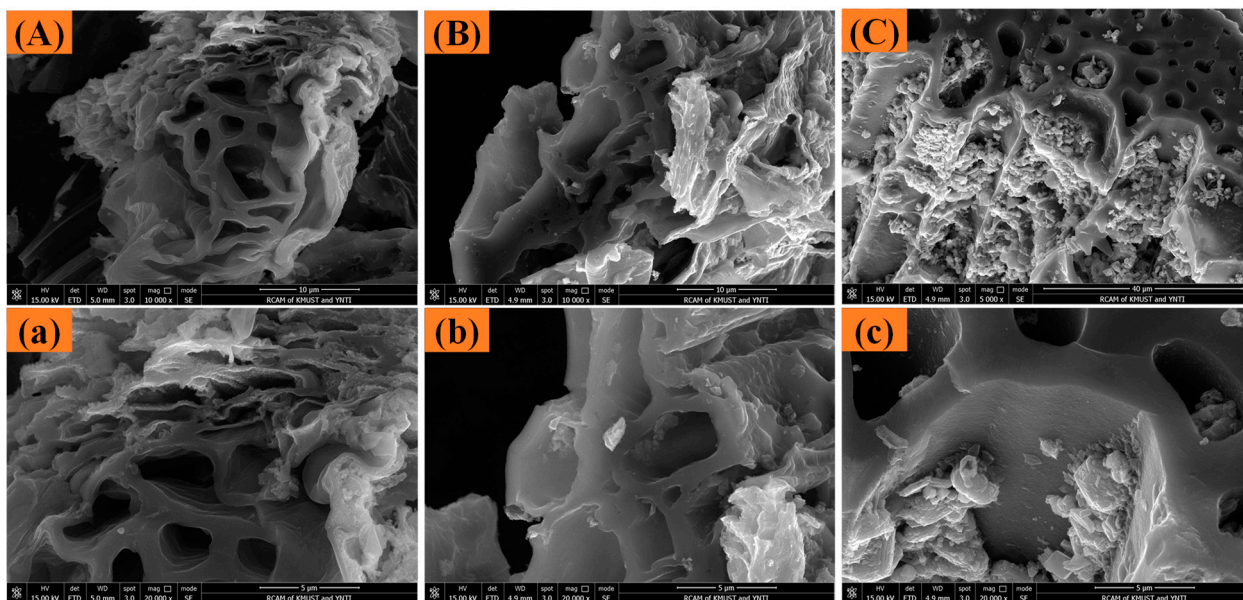


Figure 1. SEM images of PBC (A,a), MBC (B,b), and BMBC (C,c).

As presented in Table 1, the BET SSA of MBC (272.565 m²/g) is approximately twice that of PBC (123.079 m²/g), accompanied by an increase in its total pore volume to 0.173 m³/g. By contrast, BMBC exhibits a smaller BET SSA and total pore volume compared to the other two adsorbents, which can be attributed to the partial blockage of its pores by glutaraldehyde and cysteamine during chemical modification [41,42]. The average pore diameters ranging from 2.4–5.1 nm indicate that a mesoporous structure with a small presence of microporous material predominantly characterizes all three biochar adsorbents.

Table 1. Surface properties and elemental composition of biochar.

Biochar	Surface Properties			Elemental Composition (wt.%)				
	SSA (m ² /g)	TPV (m ³ /g)	APD (nm)	C 1s	O 1s	N 1s	Fe 2p	S 2p
PBC	123.079	0.083	2.553	76.77	22.81	0.41	–	–
MBC	272.565	0.173	2.443	75.86	20.29	2.43	1.31	–
BMBC	95.595	0.117	5.034	74.27	16.08	4.49	0.83	2.66

SSA, specific surface area; TPV, total pore volume; APD, average pore diameter; –, no data.

The XRD spectra in Figure 2a exhibit similar diffraction peaks at 30.10° (220), 35.45° (311), 43.08° (400), 53.45° (422), 56.98° (511), and 62.57° (440) for BMBC and MBC. This indicates the presence of Fe₃O₄ (magnetite) particles on their surfaces. Fe-based materials are known for their excellent magnetic properties, which depend on shape anisotropy and crystallinity [43]. The hysteresis curves in Figure 2b demonstrate a stronger saturation magnetization of BMBC (3.95 emu/g) compared to MBC (2.87 emu/g). Additionally, the inset picture on the bottom right of Figure 2b shows that external magnets attracted more magnetic materials in BMBC systems. These qualitative and quantitative confirmations support the successful magnetization of BMBC. The superior magnetic properties of BMBC compared to MBC can be attributed, at least partially, to the difference in crystallinity and shape anisotropy of Fe₃O₄ on the biochar surface. The chemical modification process may have strengthened the magnetization of BMBC by altering the crystallinity of Fe₃O₄.

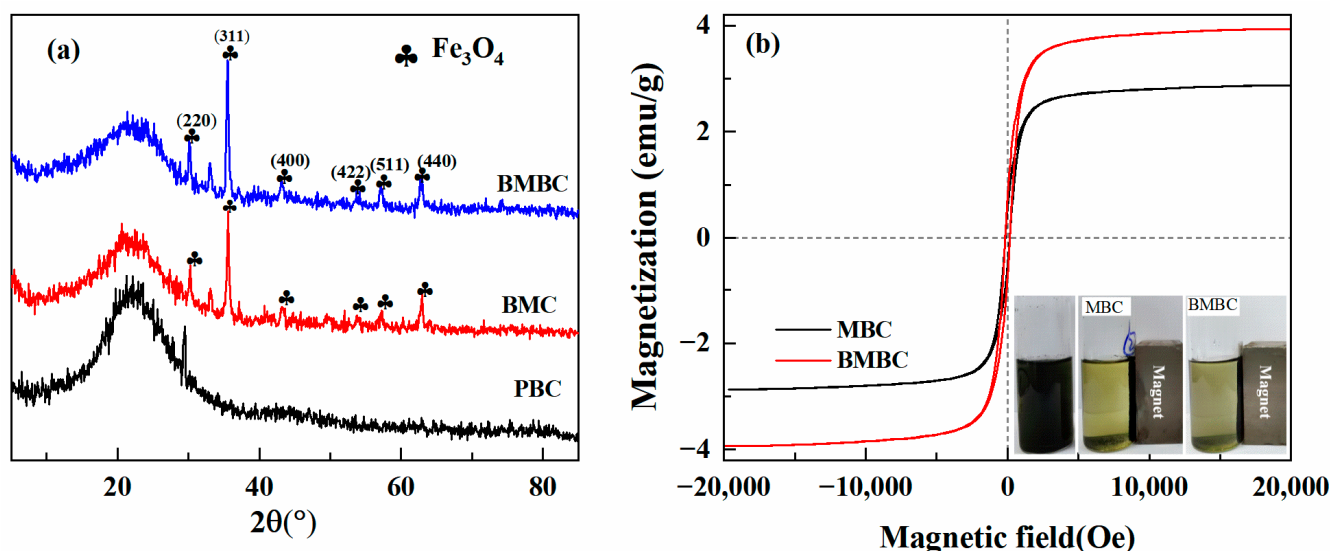


Figure 2. Spectra of XRD (a) and SVM, (b) analysis on biochar adsorbents.

The FTIR analysis in Figure 3a revealed similar peaks among the three adsorbents. For instance, a peak at 3432 cm⁻¹ corresponded to stretching vibrations of O-H and N-H, and peaks at 2924 cm⁻¹ and 2856 cm⁻¹ represented symmetrical and asymmetrical stretching vibrations of C-H in methylene [44,45]. Other similar peaks at 1594 cm⁻¹ (C-H) and 1096 cm⁻¹ (C-O) [46] were also observed. Notably, a band near 561 cm⁻¹, corresponding to Fe-O stretching vibrations, was only present in BMBC and MBC, confirming the successful loading of Fe₃O₄ [33,47]. The peaks at 1150 cm⁻¹ (C-O) and 1110 cm⁻¹ (C-N-H) were weaker in BMBC, potentially due to partial coverage of the surface by cystamine [48]. In addition, a weaker peak at 706 cm⁻¹ in BMBC may be attributed to stretching vibrations of C-S [49].

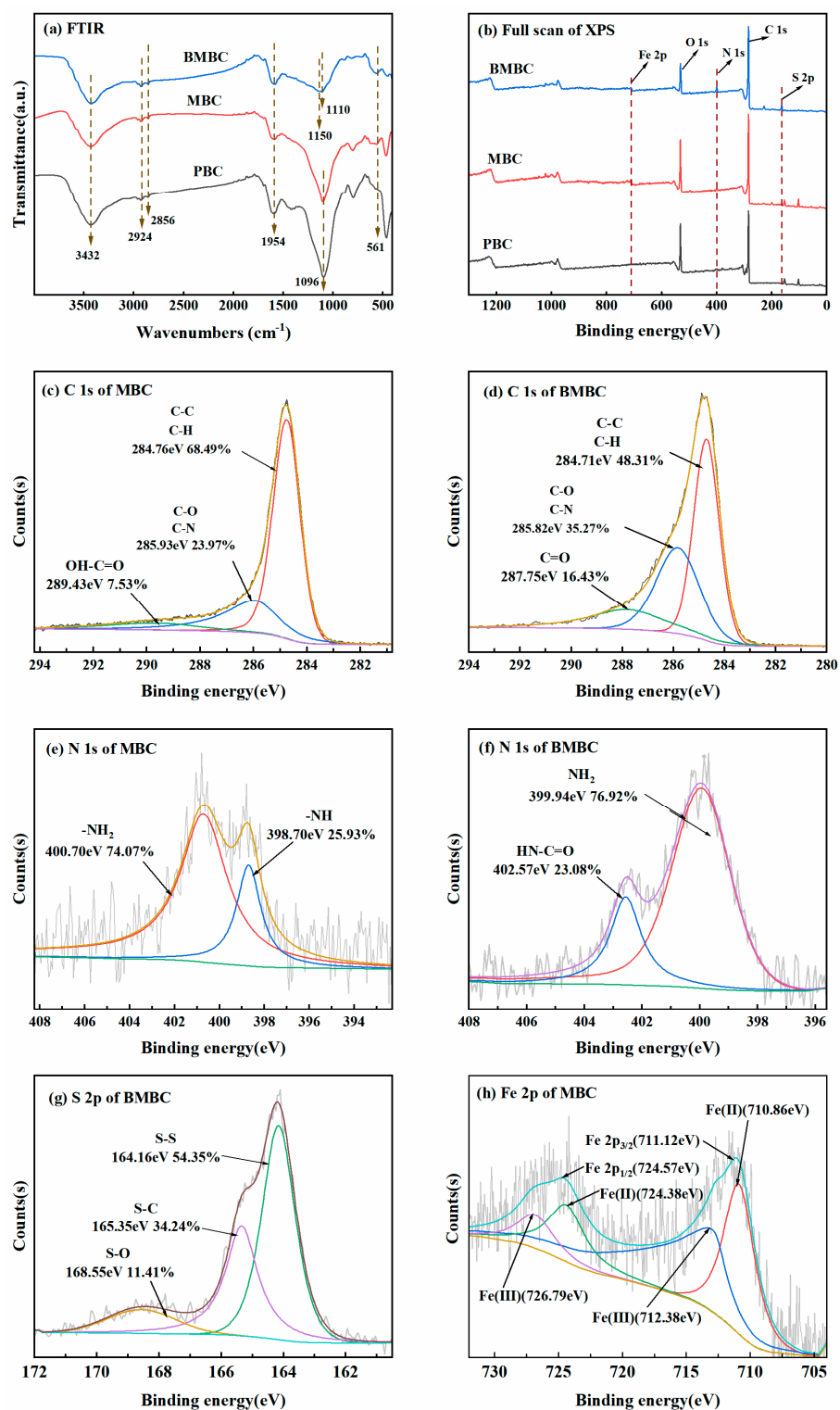


Figure 3. FTIR and XPS analysis of carbon adsorbents, including FTIR analysis (a), full-scanned XPS spectra of three biochar adsorbents (b), C 1s of MBC (c) and BMBC (d), N 1s of MBC (e) and BMBC (f), S 2p of MBC (g) and Fe 2p of MBC (h).

The full-scan XPS spectra in Table 1 and Figure 3b provided further insights. PBC was mainly composed of C 1s (76.77%) and O 1s (22.81%), with a small amount of N 1s (0.41%). MBC and BMBC exhibit increased Fe 2p signals, while BMBC also shows an elevated S 2p peak. Comparing BMBC with MBC, the C 1s and N 1s percentages increased by 3.30% and 2.06%, respectively (Table 1). The C 1s spectra of MBC (Figure 3c) displayed peaks at

284.75 eV (C-H/C-C), 285.90 eV (C-O/N), and 289.02 eV (HO-C=O) [50,51]. In contrast, the C 1s spectrum of BMBC (Figure 3d) exhibits peaks at 284.71 eV (C-H/C), 285.82 eV (C-O/N), and 287.80 eV (N-C=O) [16,52].

As depicted in Figure 3f, peaks at 399.94 eV and 402.57 eV confirm the presence of functional groups of -NH₂ and N-C=O [52]. The S 2p spectrum of BMBC shows peaks at 164.16 eV, 165.35 eV, and 168.55 eV, confirming the presence of S-S, C-S, and S-O [50,53]. The increased Fe 2p signals in BMC and BMBC (Table 1) further confirm the successful loading of Fe₃O₄ particles. The Fe 2p spectrum of MBC in Figure 3h could be deconvoluted into two primary peaks at 711.12 eV and 724.57 eV with an interval of 13.45 eV, indicating the presence of Fe₃O₄. The remaining relatively weaker peaks (710.86 eV and 724.38 eV) are assigned to Fe(II), while the others (712.38 eV and 726.79 eV) pertain to Fe(III) [54]. This is consistent with prior research data on se peaks and prior research data on Fe₃O₄ [49,54]. Overall, the FTIR and XPS analyses confirmed the successful grafting of amino, disulfide, and ester functional groups onto the surface of BMBC, with Fe₃O₄ magnetic particles adhering to MBC and BMBC.

3.2. Determinantal Factors for Cr(VI) Sorption

3.2.1. Impacts of Reaction Time and Kinetic Study

As observed in Figure 4a, the removal rate of Cr(VI) by BMBC exhibits a rapid increase in the first 720 min, followed by a ground increase from 97.9% to 100.0% with longer reaction times. In comparison, BMBC demonstrated a higher removal rate (100.0%) compared to MBC (72.37%) and PBC (61.42%). Notably, in the BMBC system, the removal rate sharply rose to 62.87% within the first 5 min and steadily ascended to 100% around 720 min, indicating complete elimination of the adsorbates from the solution. These experiment results strongly supported the efficacy of BMBC, with its amino and sulfur functional groups, in efficiently removing Cr(VI) from wastewater.

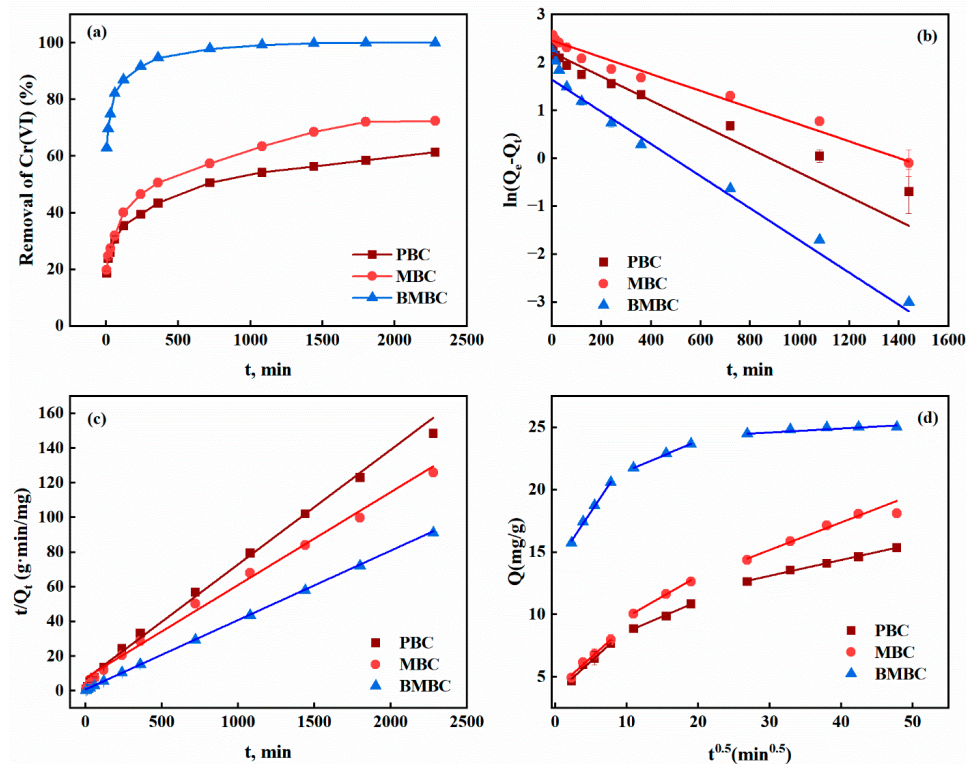


Figure 4. (a) Effect of reaction time on removal efficiency of Cr(VI) by adsorbents ($C_0 = 50$ mg/L, pH = 2, T = 30 °C); (b) sorption kinetics of Cr(VI) fitted by a pseudo-first-order model; (c) sorption kinetics of Cr(VI) fitted by a pseudo-second-order model; (d) intra-particle diffusion model plot of kinetic data for Cr(VI) adsorption.

In line with previous literature [53], the pseudo-second-order model provided a better fit for kinetics data than the pseudo-first-order model, as indicated by the higher R^2 values for the tested adsorbents (Table 2). This suggests that the sorption process is predominantly driven by chemical adsorption [55], involving electron sharing and the formation of chemical bonds [56]. Typically, the adsorption of adsorbates from solution to adsorbents involves three stages: (I) boundary layer diffusion, which transports the adsorbates from the solution onto the surface of adsorbents; (II) intra-particle diffusion, which transfers adsorbates from the surface to the interior particles of adsorbents; and (III) adsorption equilibrium, which repairs the adsorption reaction occurring on the active sites distributed within the interior particles of the adsorbents [45,55,57]. It is worth noting that the adsorption equilibrium usually affects little on the overall adsorption rate. Similar to the prior finding [15], the intra-particle diffusion model exhibited multi-curves in the kinetic data (Figure 4d), providing support for the existence of three distinct stages of Cr(VI) adsorption.

Table 2. Kinetic parameters of pseudo-first-order model and pseudo-second-order model.

Biochar Adsorbents	Pseudo-First-Order Model			Pseudo-Second-Order Model		
	K_1 (min ⁻¹)	Q_e (mg/g)	R^2	K_2 (g/(mg·min))	Q_e (mg/g)	R^2
PBC	0.0025	9.12	0.9497	0.0007	15.12	0.9970
MBC	0.0018	11.69	0.9918	0.0004	18.67	0.9929
BMBC	0.0034	5.18	0.9534	0.0022	24.98	0.9997

Table 3 consistently demonstrates a decline in the adsorption rate constant for Cr(VI) from the first stage (K_{p1}) to the third stage (K_{p3}) for all the test adsorbents. The highest K_{p1} values indicate a fast diffusion step related to the external mass transport of Cr(VI) from solution onto the adsorbent’s surface, with diffusion rate constants of 0.8592 mg/g·min^{1/2} (BMBC), 0.5167 mg/g·min^{1/2} (MBC), and 0.5177 mg/g·min^{1/2} (PBC), respectively. The slower diffusion at longer reaction times can be attributed to the mass transfer into the interior particles of the adsorbents, with respective K_{p2} values of 0.2511 mg/g·min^{1/2} (BMBC), 0.3282 mg/g·min^{1/2} (MBC), and 0.2450 mg/g·min^{1/2} (PBC). The diffusion rate constants of K_{p2} decrease in the second stage due to increased resistance to the internal diffusion of Cr(VI). Subsequently, in the third stage, the diffusion rate constant of K_{p3} continues to decrease until reaching adsorption equilibrium due to the decreasing concentration of Cr(VI) in the solution. Notably, the non-zero value of C_1 obtained from the simulated results in the first stage suggests that boundary layer diffusion does not solely control this stage of adsorption. The higher values of R^2 than 0.93 indicate that intra-particle diffusion is suitable to describe the experimental data and acts as the rate-limiting step in the second stage. At the last stage, the intra-particle diffusion begins to slow down with a decrease in the concentration of Cr(VI) in the solution, resulting in an extremely low mass transfer rate [45]. In summary, our study found that the adsorption of Cr(VI) is not solely controlled by intra-particle diffusion as the rate-limiting step but may also be affected by boundary layer diffusion [57].

Table 3. Kinetics parameters of the inter-particle diffusion model.

Biochar Adsorbents	K_{p1} (mg/g·min ^{1/2})	C_1	$(R_1)^2$	K_{p2} (mg/g·min ^{1/2})	C_2	$(R_2)^2$	K_{p3} (mg/g·min ^{1/2})	C_3	$(R_3)^2$
PBC	0.5177	3.68	0.9823	0.2450	6.18	0.9975	0.1270	9.29	0.9927
MBC	0.5167	3.99	0.9961	0.3282	6.54	0.9939	0.2210	8.55	0.9626
BMBC	0.8592	13.96	0.9966	0.2511	18.98	0.9975	0.0317	23.62	0.9343

3.2.2. Impacts of Initial Cr(VI) Concentration and Isotherm Models

The initial concentration of adsorbates is important to overcome the solid–liquid boundary’s mass transfer resistance during the transfer of Cr(VI) from the solution to the adsorbents [45]. Figure 5a showed an ascending trend in the adsorption capacity as the initial Cr(VI) concentration increased until reaching the respective upper limits of BMBC (65.82 mg/g), MBC (36.63 mg/g), and PBC (31.56 mg/g). The higher adsorption capacity of MBC compared to PBC can be attributed, at least in part, to the additional binding sites provided by the increased SSA. Despite having approximately one-third the SSA of MBC, BMBC demonstrated a greater adsorption capacity for Cr(VI) due to the presence of amino groups and sulfur bonds on its surface, which enable electrostatic interaction and complexation, enhancing its ability to adsorb Cr(VI).

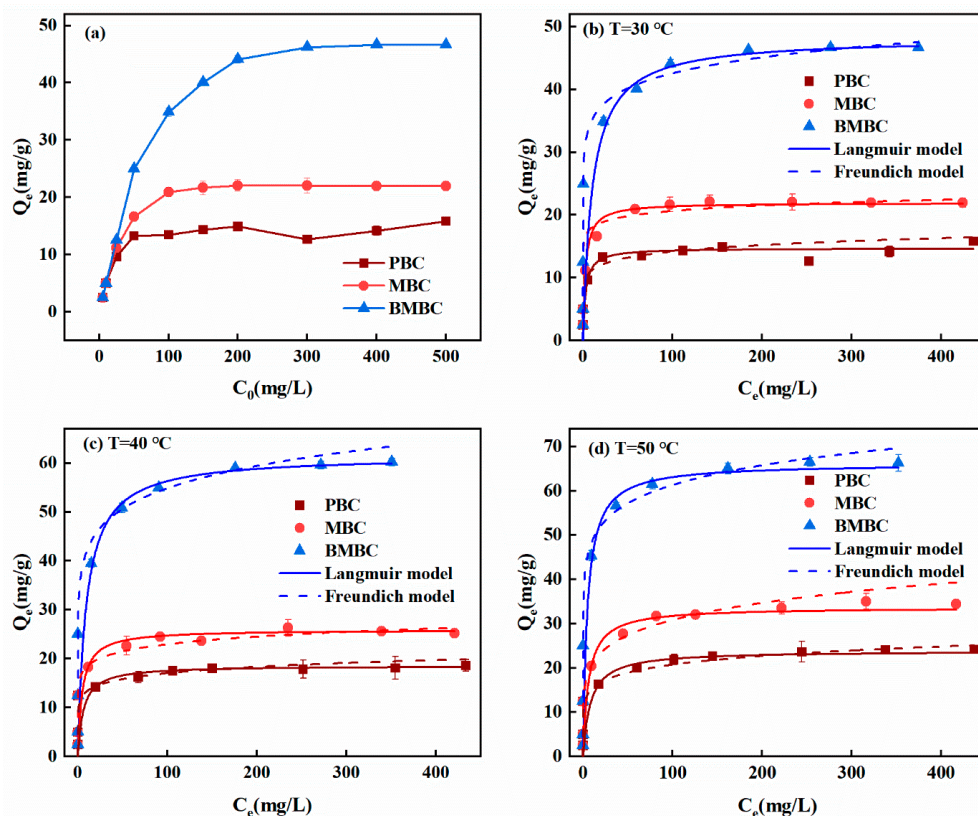


Figure 5. (a) Effect of initial Cr(VI) concentration on Cr(VI) adsorption onto adsorbents ($T = 30\text{ }^{\circ}\text{C}$, $\text{pH} = 2$, $t = 1440\text{ min}$); (b) adsorption isotherms of Cr(VI) by adsorbents at $30\text{ }^{\circ}\text{C}$; (c) adsorption isotherms of Cr(VI) by adsorbents at $40\text{ }^{\circ}\text{C}$; (d) adsorption isotherms of Cr(VI) by adsorbents at $50\text{ }^{\circ}\text{C}$.

According to Figure 5b–d and Table 4, the Langmuir model is more suitable for fitting the isotherm than the Freundlich model, as indicated by the larger values of R^2 . The Langmuir curve of BMBC shows a consistent maximum adsorption capacity of Cr(VI), which agrees well with experimental values (Figure 5b–d). The superior adsorption capacity of BMBC can be attributed to the reaction between Cr(VI) and the introduced functional groups, including iron, amino group, and disulfide bonds. The calculated R_L of BMBC declines from 0.0201 to 0.0095 when the initial Cr(VI) concentration of Cr(VI) increases from 10 mg/L to 500 mg/L at $30\text{ }^{\circ}\text{C}$, $40\text{ }^{\circ}\text{C}$, and $50\text{ }^{\circ}\text{C}$ (Table 4). This confirms that BMBC is the optimal adsorbent for removing Cr(VI). As described herein, the Langmuir model provides a better fit for experimental isotherm data in our study, and the availability of binding sites and functional groups on the surface of adsorbents limits the one-way chemical adsorption.

Table 4. Fitting parameters of adsorption isotherms of Cr(VI) by PBC, MBC, and BMBC.

Biochar	T (°C)	Langmuir			Freundlich			
		Q _{max} (mg/g)	K _L (L/mg)	R ²	R _L	n	K _F (mg/g)	R ²
PBC	30	14.69	0.3660	0.9472	0.0054	9.8880	8.885	0.8556
	40	18.55	0.1686	0.9384	0.0117	9.4930	10.4896	0.6474
	50	23.82	0.1228	0.9206	0.0160	7.6889	11.3924	0.7687
MBC	30	21.91	0.2175	0.9950	0.0091	11.9588	12.7263	0.6822
	40	25.89	0.2101	0.9651	0.0094	10.5480	14.8270	0.8152
	50	33.63	0.2670	0.9353	0.0074	5.8802	14.9895	0.9127
BMBC	30	48.19	0.0975	0.9518	0.0201	12.0097	29.0117	0.9481
	40	61.49	0.1085	0.9181	0.0181	8.6828	32.2779	0.8947
	50	66.10	0.2078	0.9278	0.0095	9.9235	38.5484	0.8618

3.2.3. Impacts of Temperature and Thermodynamic Fitting

As observed in Figure 6a, the capacities for Cr(VI) adsorption rise with an increase in temperature. Higher temperatures facilitate the diffusion of Cr(VI) in the solution and mitigate the resistance to adsorption on the adsorbents, resulting in a slight increase in adsorption capacity. The linear relationship between $\ln K_d$ and $1/T$ is observed in Figure 6b, and the fitted parameters are summarized in Table 5. The negative values of ΔG° at given temperatures indicate a spontaneous adsorption process, and the more negative ΔG° at higher temperatures suggests a greater degree of spontaneity. The positive values of ΔH° confirm an endothermic adsorption process, while the positive ΔS° reflects the increased randomness between the solid–liquid interface [45,58]. These findings indicate that Cr(VI) adsorption occurs spontaneously and endothermically. Moreover, adsorption capacities are enhanced at higher temperatures.

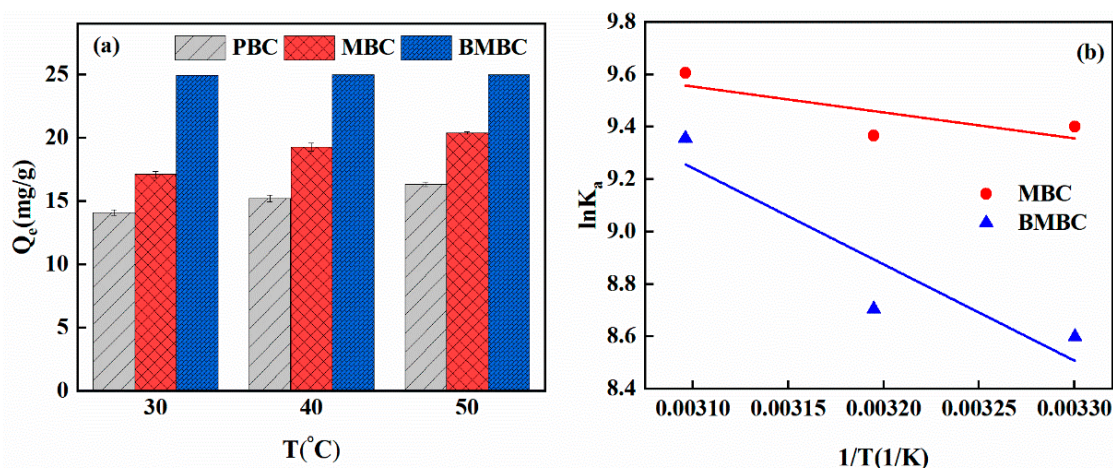


Figure 6. (a) Impact of temperature on Cr(VI) adsorption for three biochar adsorbents (C₀ = 50 mg/L, pH = 2, t = 1440 min); (b) thermodynamic plots of Cr(VI) adsorption for MBC and BMBC.

Table 5. Thermodynamics parameters for Cr(VI) adsorbed by MBC and BMBC.

Adsorbents	T (K)	ΔG° (kJ/mol·K)	ΔS° (J/mol·K)	ΔH° (kJ/mol·K)
MBC	303 (30 °C)	−17.09	58.55	0.51
	313 (40 °C)	−18.12		
	323 (50 °C)	−18.24		
BMBC	303 (30 °C)	−15.60	70.57	5.70
	313 (40 °C)	−16.58		
	323 (50 °C)	−17.00		

3.2.4. Impact of pH in Solution

Solution pH is a critical determinant for removing heavy metal ions as it affects both the solution's ionic form and the adsorbents' surface properties [47,59]. As shown in Figure 7a, the maximum percentage of Cr(VI) was removed when the solution pH was 2. Among them, BMBC exhibits much higher Cr(VI) removal efficiency (98.81%) compared to MBC (69.13%) and PBC (57.06%). The removal efficiencies of Cr(VI) were negatively related to solution pH, which is attributed, at least in part, to the surface characteristics of adsorbents [44]. Figure 7b showed a rapid decrease in the positive zeta potential as the solution pH rose from 2 to 4, followed by a gentle decline until reaching the minimum value of 32.93 mV in the BMBC system, implying abundant positive charges on its surface. This suggests that the surface of BMBC presents abundant positive charges that can easily bind with Cr(VI) anions through electrostatic interactions. In an acidic environment, Cr(VI) is predominantly present in the forms of HCrO_4^- and $\text{Cr}_2\text{O}_7^{2-}$, while it exists as CrO_4^{2-} in neutral and alkaline environments [60]. Alkaline functional groups on the surface of adsorbents can undergo protonation under acidic conditions, leading to the formation of positive charges [30], which are capable of binding solution Cr(VI) anion to the surface of adsorbents through electrostatic interaction. Similarly, the $-\text{NH}_2$ group on the BMBC surface can be protonated, creating additional sites [30]. On the other hand, disulfide bonds (S-S) can be cleaved, forming mercaptan groups that enable the coordination and immobilization of Cr(VI) ions [61]. This mechanism makes BMBC exhibit enhanced Cr(VI) removal at low pH levels. Despite having equal zeta potentials, the presence of Fe_3O_4 particles on the surface of MBC contributes to a higher removal rate of Cr(VI) compared to PBC [62].

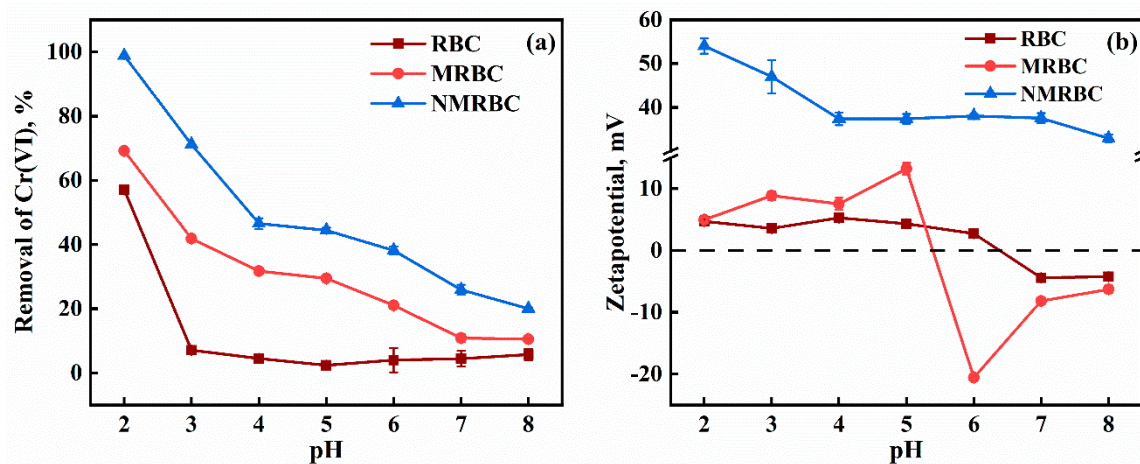


Figure 7. (a) Impact of pH on Cr(VI) removal by adsorbents; (b) zeta potential of adsorbents depending on pH values ($C_0 = 50 \text{ mg/L}$, $t = 1440 \text{ min}$, $T = 30 \text{ }^\circ\text{C}$).

3.2.5. Impacts of Co-Existing Ions

Other co-existing ions in wastewater can compete for surface binding sites with Cr(VI), reducing adsorption capacity [63]. To investigate the impacts of these ions on Cr(VI) removal, additional experiments were carried out using a prepared solution containing a mixed concentration of 50 mg/L for Cr(VI), Cu(II), Mn(II), Cd(II), and K(I), with a separate pure solution of 50 mg/L Cr(VI) as a reference (Cr(VI)-0). As shown in Figure 8a, BMBC exhibits an excellent Cr(VI) removal efficiency of 96.37% but much lower eliminate rates for other co-existing cations such as Cu(II) (15.27%), Cd(II) (10.50%), Mn(II) (9.76%), and K(I) (4.60%), suggesting its better specificity for Cr(VI) removal. However, there is a decrease in the percentage of Cr(VI) removal in MBC (8.17%) and PBC (6.79%) compared to that of BMBC (3.63%) in mixed systems, indicating the existence of competitive adsorption between Cr(VI) and other metal cations. At a pH level of 2, the positive charges on the

BMBC surface can produce electrostatic repulsion with other cations and selectively bind with the Cr(VI) anion.

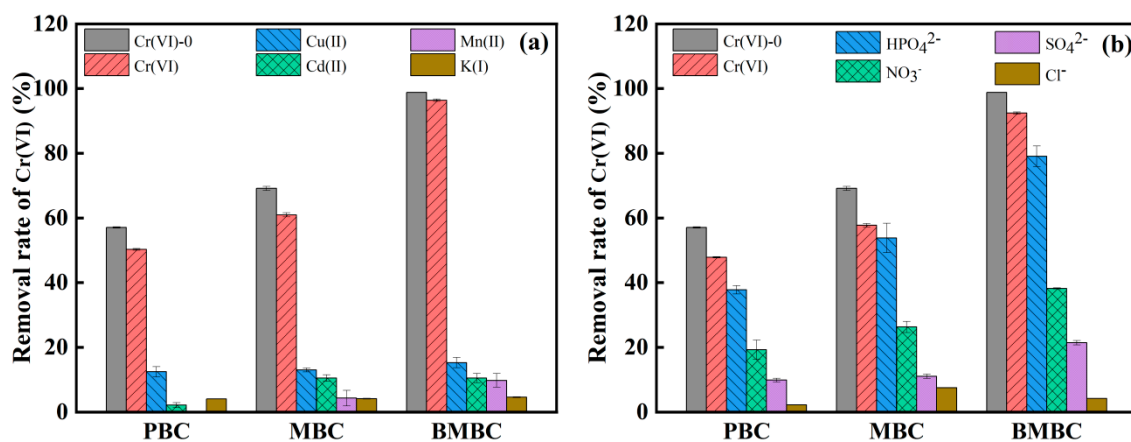


Figure 8. Impacts of co-existing cations (a) and anions (b) on Cr(VI) removal.

The impacts of four common anions (i.e., Cl^- , NO_3^- , SO_4^{2-} , and HPO_4^{2-}) on Cr(VI) removal were illustrated in Figure 8b. Although the Cr(VI) removal rate of BMBC decreased by 7.58% in the presence of co-existing anions compared to the reference, it remained at 92.42% due to its remarkable specificity to Cr(VI). Co-existing anions may hinder the electrostatic interaction between Cr(VI) adsorbents by competing for active sites with Cr(VI).

3.3. Mechanism Underlying Sorption

XPS spectra (Figure 9a) after adsorption revealed the emergence of a new band corresponding to Cr 2p. The Cr 2p spectra of BMBC (Figure 9b) exhibited two peaks at 587.28 eV (Cr 2p_{1/2}) and 577.28 eV (Cr 2p_{3/2}), with the Cr 2p_{3/2} peak comprising Cr(VI) (578.45 eV) and Cr(III) (577.05 eV) [38,60]. These peaks provide evidence that the adsorbed Cr(VI) on the BMBC surface was partially reduced to Cr(III). The Fe 2p spectra of BMBC (Figure 9c) exhibit two peaks at 723.63 eV and 709.63 eV that can be assigned to Fe₂O₃. However, Fe₂O₃ was not observed in the XRD analysis. One possible explanation is that the generated Fe₂O₃ was very low and thus could not be detected [6,64]. The peaks of Fe 2p_{3/2} were shifted to 710.86 eV (Fe(II)) and 712.90 eV (Fe(III)), and a new peak appeared at 711.30 eV, along with a satellite peak at 718.08 eV, which corresponds to FeCr₂O₄ and Fe(III), respectively [6,54]. This result suggests that a portion of Fe(II) was oxidized to Fe(III). Accordingly, an oxidation–reduction reaction occurred between Cr(VI) and Fe₃O₄ on the adsorbent surface, resulting in a partial reduction of Cr(VI) to Cr(III).

Comparison of the C 1s spectra of BMBC before (Figure 3d) and after (Figure 9d) adsorption showed that the percentage of C-H/C decreased from 48.31% to 44.84% and that of N-C=O decreased from 16.43% to 15.70%. Conversely, the percentage of C-O increased from 35.27% to 39.46%. The phenomenon can be attributed to the participation of active surface groups such as ester, which are capable of reducing Cr(VI) to Cr(III) by providing electrons [65]. The N 1s spectrum of BMBC after Cr(VI) absorption (Figure 9e) exhibited a slight shift in the peaks corresponding to -NH₂ and HN-C=O, especially a 22.28% reduction in the -NH₂ peak. This peak shift and percentage reduction can be explained by the protonation of surface amino groups into -NH₃⁺ and the subsequent formation of a chromium complex (Cr(III)-N) through electrostatic interaction with Cr(VI) [60]. Additionally, a new peak assigned to nitrate was observed at 406.72 eV, indicating the reaction of BMBC surface groups with Cr(VI) and the formation of a nitrate-like substance to (Cr(III)-N-O) [52]. The S 2p spectrum of BMBC after absorbing Cr(VI) (Figure 9f) provided evidence that the disulfide bond (S-S) can reduce Cr(VI) into Cr(III) via redox reaction, which shifted the S-S peak and lessened its proportion [66].

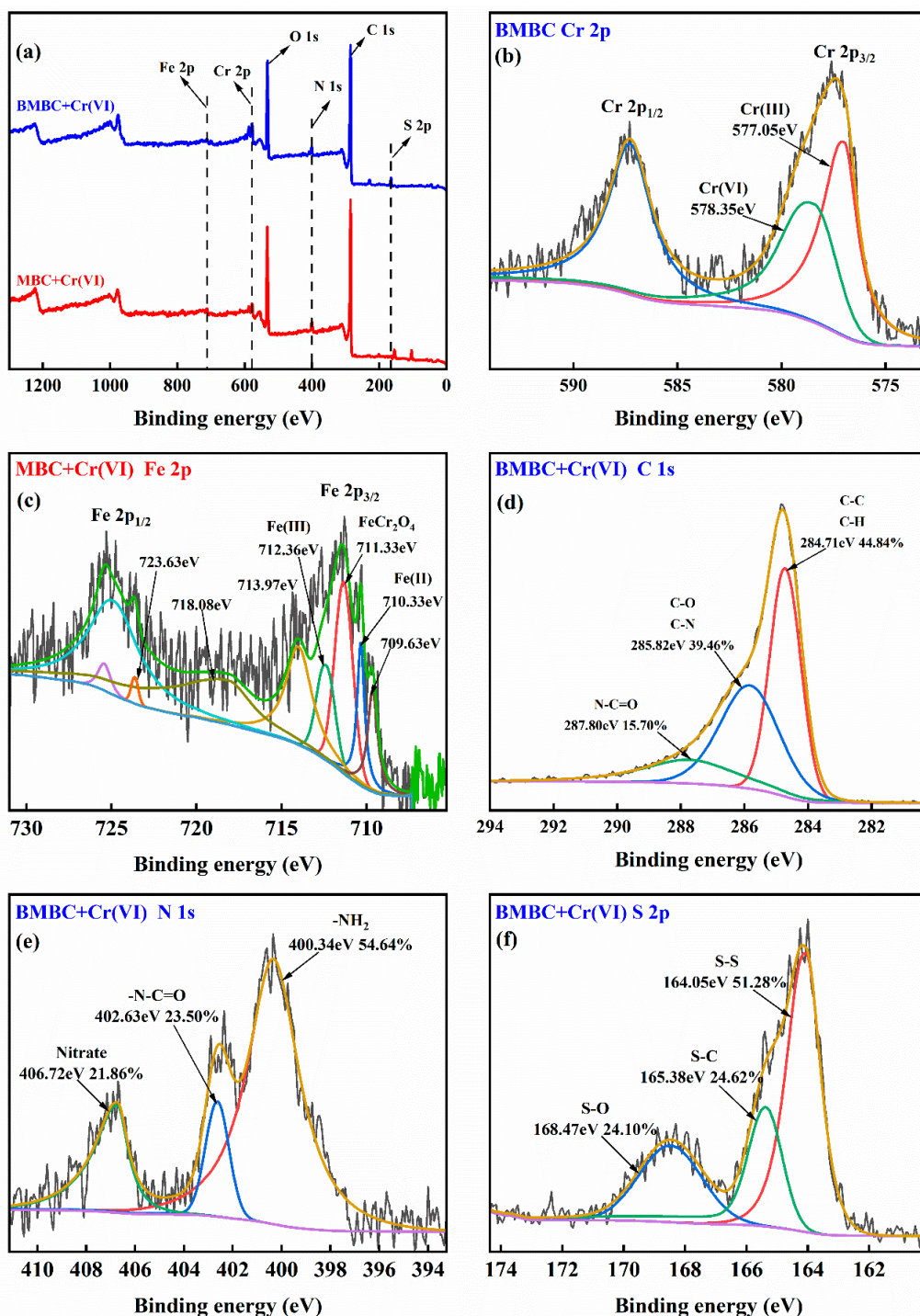


Figure 9. XPS spectra of adsorbents after adsorption. (a) full scan; (b) Cr 2p; (c) Fe 2p; (d) C 1s, (e) N 1s and (f) S 2p.

According to the results above, the mechanisms underlying Cr(VI) adsorption in the BMBC system can be attributed to three aspects (Figure 10). Firstly, solution Cr(VI) can transfer rapidly to the surface of BMBC through boundary-layer and intra-particle diffusion and be adsorbed onto the BMBC surface through electrostatic interactions. Secondly, a portion of adsorbed Cr(VI) can be reduced to Cr(III) and captured by a weaker acid, thus facilitating simultaneous reduction and adsorption processes for both Cr(VI) and Cr(III). Thirdly, the Cr(III) species forms complexes with surface functional groups, such as amino and ester groups, present on the BMBC surface.

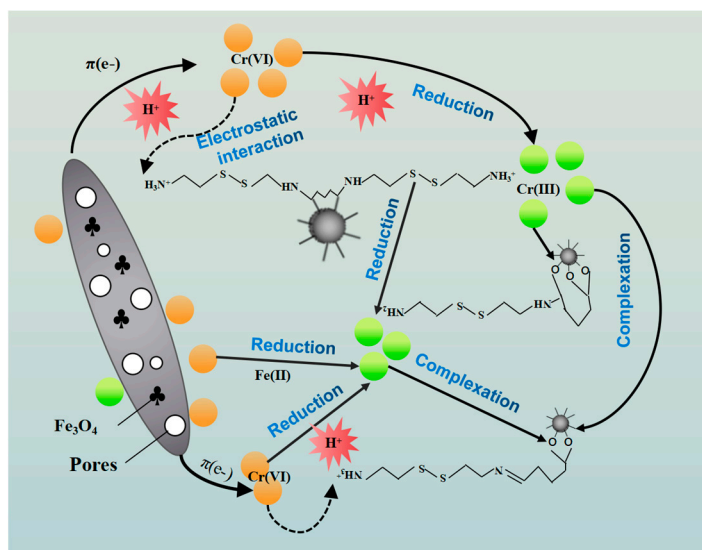


Figure 10. Underlying mechanisms for Cr(VI) removal of BMBC.

3.4. Regeneration and Re-Usability Study

Re-usability is a significant consideration in determining the application potential of an adsorbent for wastewater treatment. As revealed in Figure 11, the Cr(VI) removal rate gradually decreased with an increase in consecutive adsorption/desorption cycles for all tested adsorbents. However, BMBC demonstrated superior performance in Cr(VI) removal compared to BMC and PBC. In the BMBC system, the Cr(VI) removal rate remained at 61.12% after the fifth regeneration cycle, which is comparable to the maximum Cr(VI) removal rate of PBC. Accordingly, this novel BMBC is stable and reusable for treating Cr(VI) in wastewater.

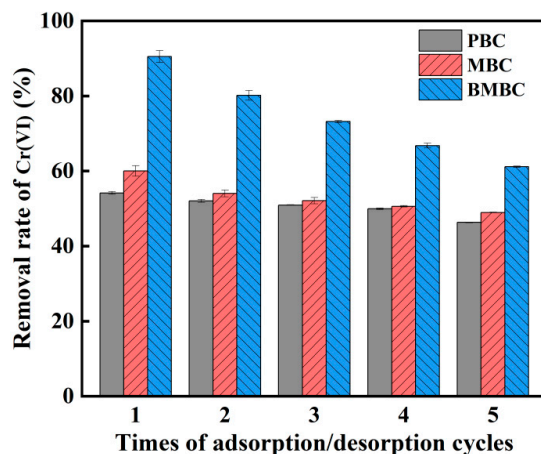


Figure 11. Removal performance of Cr(VI) by adsorbents during five consecutive adsorption/desorption cycles.

3.5. Comparing Adsorption Capacity of Cr(VI)

As summarized in Table 6, the maximum adsorption capacity of BMBC is 66.10 mg/g, which is nearly double that of MBC and higher than the capacities reported for many other chemically modified crop straw adsorbents in previous studies (Table 6). These findings suggest that BMBC is an efficient and promising magnetic adsorbent for Cr(VI). This observation is consistent with the results of other studies [32,66,67], which have also demonstrated that surface modification of biochar using cystamine is an effective method to fabricate super adsorption materials for Cr(VI).

Table 6. Comparison of the Cr(VI) removal capacity of BMBC with other chemically modified crop straw biochar.

Reference	Carbon Source	Biochar	Modifying Agent	Sorption Capacity (mg/g)	Magnetism	Temperature (°C)	Solution pH
This work	Rice straw	BMBC	Cystamine, glutaraldehyde	66.10	Yes	50	2
		BMC	Fe(III)/Fe(II) mixture	33.63	Yes	50	2
		PBC	Raw	23.82	Yes	50	2
[34]	Rice straw	BC-G1	HNO ₃ , G1 polyamidoamine dendrimer	101.52	No	30	2
		BC-G2	HNO ₃ , G2 polyamidoamine dendrimer	120.77	No	30	2
		BC-G3	HNO ₃ , G3 polyamidoamine dendrimer	40.98	No	30	2
[67]	Rice straw	A-RS/PVA	Amination reaction: polyvinyl alcohol and diethylenetriamine	142.03	No	60	2
[11]	Rice straw	WS-CA-AM	NaOH, citric acid, acrylamide	53.88	No	25	3
[11]	Rice straw	MRS	Amine-functionalization: epichlorohydrin, diethylenetriamine	21.87	No	25	2
[66]	Rice straw	Fe ₃ O ₄ -PEI-SERS	Amino-functionalization: polyethyleneimine, Fe ₃ O ₄	338.98	Yes	45	2
[32]	Wheat straw	AC-WS	Amination reaction: epichlorohydrin and ethylenediamine	287.02	No	30	2
[68]	Corn stalks	MCS	Amine-functionalization: epichlorohydrin, diethylenetriamine	194.13	No	25	4
[69]	Corn straw		HNO ₃ activation	33.33	No	/	~7
[30]	Peanut shells	PHC-HDA	Amino-functionalized magnetic biochar using hexamethylenediamine (HDA)	121.95	No	25	2
		MPHC-HDA	HDA-modified magnetic biochar	142.86	No	25	2

4. Conclusions

Modification of BMC using cystamine, which contains abundant amino groups and disulfide bonds, improved Cr(VI) removal efficacy. The results confirmed that BMBC exhibited a higher percentage of Cr(VI) removal (100%) compared to MBC (72.37%) and PBC (61.42%). The maximum removal of Cr(VI) was achieved at a solution pH of 2 for all three biochar adsorbents. The optimal reaction time and initial adsorbate concentration for Cr(VI) removal were determined to be 1440 min and 300 mg/L, respectively. The higher fitting values obtained from the Langmuir model indicated that the adsorption followed a monolayer adsorption process, with a maximum adsorption capacity of 66.10 mg/g at 50 °C and pH of 2. The better-fitting values obtained for the pseudo-second-order kinetics suggested a chemical adsorption process. The positive values of ΔH° and ΔS° and the negative value of ΔG° indicated that the Cr(VI) adsorption was spontaneous, endothermic, and characterized by high randomness at the solid/liquid interface. The potential mechanisms underlying the adsorption involved electrostatic interactions between Cr(VI) in the solution and the positive charges on the adsorbent surface. Additionally, the introduced amino, sulfur, and Fe(II) groups facilitate the reduction of adsorbed Cr(VI) to Cr(III). Subsequently, complexation occurs between the reduced Cr(III) species and functional groups present on the adsorbent surface. In the presence of co-existing cations such as Cu(II), Cd(II), Mn(II), and K(I), the Cr(VI) removal efficacy was minimally affected. In contrast, the presence of certain anions, such as Cl⁻, NO₃⁻, SO₄²⁻, and HPO₄²⁻, resulted in a 7.58% decrease in the removal rate of Cr(VI). After undergoing five consecutive

adsorption/desorption cycles, BMBC still exhibited a high Cr(VI) removal rate of 61.12%. Overall, this novel BMBC derived from rice straw shows promising potential as a bio-sorbent for treating Cr(VI) in wastewater.

Author Contributions: All authors contributed to this work. Specifically, J.L. and M.L. designed the experiments. J.W. conducted the batch experiments, and Q.Z. performed the characterization. X.C. interpreted the data and worked out the manuscript. J.H., X.H., and C.L. advised on the conception and design of the study, as well as on the revision of the manuscripts. All authors have read and agreed to the published version of the manuscript.

Funding: This research was funded by [National Natural Science Foundation of China] grant number [52060011], [the Basic Research Programs of Yunnan Province] grant number [202101AU070038] grant number [202101AT070129] and grant number [202101BE070001-024], and [Environmental Protection Technology Research Project of the Yunnan Provincial Department of Ecology and Environment] grant number (YNJH2019224).

Institutional Review Board Statement: Not applicable.

Informed Consent Statement: Not applicable.

Data Availability Statement: All related data are included in the present paper or available upon request.

Conflicts of Interest: The authors declare no conflict of interest.

References

1. Pradhan, D.; Sukla, L.B.; Sawyer, M.; Rahman, P.K.S.M. Recent bioreduction of hexavalent chromium in wastewater treatment: A review. *J. Ind. Eng. Chem.* **2017**, *55*, 1–20. [[CrossRef](#)]
2. Qiao, K.; Tian, W.; Bai, J.; Zhao, J.; Du, Z.; Song, T.; Chu, M.; Wang, L.; Xie, W. Synthesis of floatable magnetic iron/biochar beads for the removal of chromium from aqueous solutions. *Environ. Technol. Innov.* **2020**, *19*, 100907. [[CrossRef](#)]
3. IARC (International Agency for Research on Cancer). List of Classifications—IARC Monographs on the Identification of Carcinogenic Hazards to Humans. Last Updated: 2022-09-07 10.34am (CEST). Available online: https://monographs.iarc.who.int/wp-content/uploads/2019/07/Classifications_by_cancer_site.pdf (accessed on 5 May 2023).
4. Costa, M.; Klein, C.B. Toxicity and carcinogenicity of chromium compounds in humans. *Crit. Rev. Toxicol.* **2006**, *36*, 155–163. [[CrossRef](#)]
5. Zhang, W.; Long, A.; Ou, J.; Zeng, X.; Wang, J.; Wang, B.; Wang, H.; He, Q.; Tang, M.; Zhou, L.; et al. Enhanced removal of hexavalent chromium from aqueous solution by functional polymer-wrapped gamma-alumina composite adsorbent. *Environ. Technol. Innov.* **2021**, *24*, 101954. [[CrossRef](#)]
6. Zhong, D.; Zhang, Y.; Wang, L.; Chen, J.; Jiang, Y.; Tsang, D.C.; Zhao, Z.; Ren, S.; Liu, Z.; Crittenden, J.C. Mechanistic insights into adsorption and reduction of hexavalent chromium from water using magnetic biochar composite: Key roles of Fe₃O₄ and persistent free radicals. *Environ. Pollut.* **2018**, *243* (Pt B), 1302–1309. [[CrossRef](#)]
7. Pan, C.; Troyer, L.D.; Catalano, J.G.; Giammar, D.E. Dynamics of Chromium(VI) Removal from Drinking Water by Iron Electrocoagulation. *Environ. Sci. Technol.* **2016**, *50*, 13502–13510. [[CrossRef](#)]
8. Rapti, S.; Pournara, A.; Sarma, D.; Papadas, I.T.; Armatas, G.S.; Tsipis, A.C.; Lazarides, T.; Kanatzidis, M.G.; Manos, M.J. Selective capture of hexavalent chromium from an anion-exchange column of metal organic resin–alginate composite. *Chem. Sci.* **2016**, *7*, 2427–2436. [[CrossRef](#)]
9. Duan, W.; Chen, G.; Chen, C.; Sanghvi, R.; Iddya, A.; Walker, S.; Liu, H.; Ronen, A.; Jassby, D. Electrochemical removal of hexavalent chromium using electrically conducting carbon nanotube/polymer composite ultrafiltration membranes. *J. Membr. Sci.* **2017**, *531*, 160–171. [[CrossRef](#)]
10. Liu, C.; Fiol, N.; Villaescusa, I.; Poch, J. New approach in modeling Cr(VI) sorption onto biomass from metal binary mixtures solutions. *Sci. Total Environ.* **2016**, *541*, 101–108. [[CrossRef](#)] [[PubMed](#)]
11. Liu, L.; Liu, X.; Wang, D.; Lin, H.; Huang, L. Removal and reduction of Cr(VI) in simulated wastewater using magnetic biochar prepared by co-pyrolysis of nano-zero-valent iron and sewage sludge. *J. Clean. Prod.* **2020**, *257*, 120562. [[CrossRef](#)]
12. Cheng, N.; Wang, B.; Wu, P.; Lee, X.; Xing, Y.; Chen, M.; Gao, B. Adsorption of emerging contaminants from water and wastewater by modified biochar: A review. *Environ. Pollut.* **2021**, *273*, 116448. [[CrossRef](#)] [[PubMed](#)]
13. Rajapaksha, A.U.; Selvasembian, R.; Ashiq, A.; Gunarathne, V.; Ekanayake, A.; Perera, V.; Wijesekera, O.H.; Mia, S.; Ahmad, M.; Vithanage, M.; et al. A Systematic Review on Adsorptive Removal of Hexavalent Chromium from Aqueous Solutions: Recent Advances. *Sci Total Environ* **2022**, *809*, 152055. [[CrossRef](#)] [[PubMed](#)]
14. Karthikeyan, T.; Rajgopal, S.; Miranda, L. Chromium(VI) adsorption from aqueous solution by sawdust activated carbon. *J. Hazard. Mater.* **2005**, *124*, 192–199. [[CrossRef](#)] [[PubMed](#)]
15. Niu, H.Y.; Li, X.; Li, J. Dithiocarbamate modification of activated carbon for the efficient removal of Pb(II), Cd(II), and Cu(II) from wastewater. *New J. Chem.* **2022**, *46*, 5234–5245. [[CrossRef](#)]

16. Chen, H.; Gao, Y.; El-Naggar, A.; Niazi, N.K.; Sun, C.; Shaheen, S.M.; Hou, D.; Yang, X.; Tang, Z.; Liu, Z.; et al. Enhanced sorption of trivalent antimony by chitosan-loaded biochar in aqueous solutions: Characterization, performance and mechanisms. *J. Hazard. Mater.* **2022**, *425*, 127971. [[CrossRef](#)]
17. Ifthikar, J.; Chen, Z.; Chen, Z.; Jawad, A. A self-gating proton-coupled electron transfer reduction of hexavalent chromium by core-shell SBA-Dithiocarbamate chitosan composite. *J. Hazard. Mater.* **2020**, *384*, 121257. [[CrossRef](#)]
18. Nazir, M.A.; Najam, T.; Shahzad, K.; Wattoo, M.A.; Hussain, T.; Tufail, M.K.; Shah, S.S.A.; Rehman, A.U. Heterointerface engineering of water stable ZIF-8@ZIF-67: Adsorption of rhodamine B from water. *Surf. Interfaces* **2022**, *34*, 102324. [[CrossRef](#)]
19. Zhao, N.; Zhao, C.; Tsang, D.C.; Liu, K.; Zhu, L.; Zhang, W.; Zhang, J.; Tang, Y.; Qiu, R. Microscopic mechanism about the selective adsorption of Cr(VI) from salt solution on O-rich and N-rich biochars. *J. Hazard. Mater.* **2021**, *404*, 124162. [[CrossRef](#)]
20. Zou, H.; Zhao, J.; He, F.; Zhong, Z.; Huang, J.; Zheng, Y.; Zhang, Y.; Yang, Y.; Yu, F.; Bashir, M.A.; et al. Ball milling biochar iron oxide composites for the removal of chromium (Cr(VI)) from water: Performance and mechanisms. *J. Hazard. Mater.* **2021**, *413*, 125252. [[CrossRef](#)]
21. Zheng, Y.; Zimmerman, A.R.; Gao, B. Comparative investigation of characteristics and phosphate removal by engineered biochars with different loadings of magnesium, aluminum, or iron. *Sci. Total Environ.* **2020**, *747*, 141277. [[CrossRef](#)]
22. Foong, S.Y.; Chan, Y.H.; Chin, B.L.F.; Lock, S.S.M.; Yee, C.Y.; Yiin, C.L.; Peng, W.; Lam, S.S. Production of Biochar from Rice Straw and Its Application for Wastewater Remediation—An Overview. *Bioresour. Technol.* **2022**, *360*, 127588. [[CrossRef](#)] [[PubMed](#)]
23. FAOSTAT. Crops and Livestock Products. Food and Agriculture Organization of the United Nations. 2021. Available online: <https://www.fao.org/faostat/en/#data/QCL> (accessed on 24 March 2023).
24. Malik, K.; Ajay, S.; Dandu, H.; Vijaya, R.; Nisha, A.; Anurag, M.; Sunita, R.; Punesh, S.; Tanvi, B. Deciphering the Biochemical and Functional Characterization of Rice Straw Cultivars for Industrial Applications. *Heliyon* **2023**, *9*, e16399. [[CrossRef](#)] [[PubMed](#)]
25. Chen, J.; Li, C.; Ristovski, Z.; Milic, A.; Gu, Y.; Islam, M.S.; Wang, S.; Hao, J.; Zhang, H.; He, C.; et al. A review of biomass burning: Emissions and impacts on air quality, health and climate in China. *Sci. Total Environ.* **2017**, *579*, 1000–1034. [[CrossRef](#)] [[PubMed](#)]
26. Shi, W.J.; Fang, Y.R.; Chang, Y.Y.; Xie, G.H. Toward sustainable utilization of crop straw: Greenhouse gas emissions and their reduction potential from 1950 to 2021 in China. *Resour. Conserv. Recycl.* **2023**, *190*, 106824. [[CrossRef](#)]
27. Rajapaksha, A.U.; Chen, S.S.; Tsang, D.C.; Zhang, M.; Vithanage, M.; Mandal, S.; Gao, B.; Bolan, N.S.; Ok, Y.S. Engineered/designer biochar for contaminant removal/immobilization from soil and water: Potential and implication of biochar modification. *Chemosphere* **2016**, *148*, 276–291. [[CrossRef](#)]
28. Chen, R.; Zhao, X.; Jiao, J.; Li, Y.; Wei, M. Surface-Modified Biochar with Polydentate Binding Sites for the Removal of Cadmium. *Int. J. Mol. Sci.* **2019**, *20*, 1755. [[CrossRef](#)]
29. Li, H.; Dong, X.; da Silva, E.B.; de Oliveira, L.M.; Chen, Y.; Ma, L.Q. Mechanisms of metal sorption by biochars: Biochar characteristics and modifications. *Chemosphere* **2017**, *178*, 466–478. [[CrossRef](#)]
30. Cai, W.; Wei, J.; Li, Z.; Liu, Y.; Zhou, J.; Han, B. Preparation of amino-functionalized magnetic biochar with excellent adsorption performance for Cr(VI) by a mild one-step hydrothermal method from peanut hull. *Colloids Surf. A Physicochem. Eng. Asp.* **2019**, *563*, 102–111. [[CrossRef](#)]
31. Deng, J.; Li, X.; Wei, X.; Liu, Y.; Liang, J.; Shao, Y.; Huang, W.; Cheng, X. Different adsorption behaviors and mechanisms of a novel amino-functionalized hydrothermal biochar for hexavalent chromium and pentavalent antimony. *Bioresour. Technol.* **2020**, *310*, 123438. [[CrossRef](#)]
32. Xu, X.; Gao, B.Y.; Tan, X.; Yue, Q.Y.; Zhong, Q.Q.; Li, Q. Characteristics of Amine-Crosslinked Wheat Straw and Its Adsorption Mechanisms for Phosphate and Chromium (Vi) Removal from Aqueous Solution. *Carbohydr. Polym.* **2011**, *84*, 1054–1060. [[CrossRef](#)]
33. Li, F.Y.; Zimmerman, A.R.; Hu, X.; Gao, B. Removal of aqueous Cr(VI) by Zn- and Al-modified hydrochar. *Chemosphere* **2020**, *260*, 127610. [[CrossRef](#)] [[PubMed](#)]
34. Li, J.; He, J.; Huang, J.; Zhao, Q.; Li, Y.; Tian, S. Removal of Cr(VI) from aqueous solutions using polyamidoamine dendrimer-modified biochar. *Desalination Water Treat.* **2022**, *270*, 111–126. [[CrossRef](#)]
35. Shi, L.; Wang, T.; Zhang, H.; Chang, K.; Meng, X.; Liu, H.; Ye, J. An Amine-Functionalized Iron(III) Metal-Organic Framework as Efficient Visible-Light Photocatalyst for Cr(VI) Reduction. *Adv. Sci. (Weinh)* **2015**, *2*, 1500006. [[CrossRef](#)]
36. Qu, J.; Shi, J.; Wang, Y.; Tong, H.; Zhu, Y.; Xu, L.; Wang, Y.; Zhang, B.; Tao, Y.; Dai, X.; et al. Applications of functionalized magnetic biochar in environmental remediation: A review. *J. Hazard. Mater.* **2022**, *434*, 128841. [[CrossRef](#)] [[PubMed](#)]
37. Feng, Z.; Yuan, R.; Wang, F.; Chen, Z.; Zhou, B.; Chen, H. Preparation of magnetic biochar and its application in catalytic degradation of organic pollutants: A review. *Sci. Total Environ.* **2021**, *765*, 142673. [[CrossRef](#)]
38. Kera, N.H.; Bhaumik, M.; Pillay, K.; Ray, S.S.; Maity, A. Selective removal of toxic Cr(VI) from aqueous solution by adsorption combined with reduction at a magnetic nanocomposite surface. *J. Colloid Interface Sci.* **2017**, *503*, 214–228. [[CrossRef](#)]
39. Tan, X.; Liu, Y.; Zeng, G.; Wang, X.; Hu, X.; Gu, Y.; Yang, Z. Application of biochar for the removal of pollutants from aqueous solutions. *Chemosphere* **2015**, *125*, 70–85. [[CrossRef](#)]
40. Qu, J.; Meng, Q.; Lin, X.; Han, W.; Jiang, Q.; Wang, L.; Hu, Q.; Zhang, L.; Zhang, Y. Microwave-assisted synthesis of beta-cyclodextrin functionalized celluloses for enhanced removal of Pb(II) from water: Adsorptive performance and mechanism exploration. *Sci. Total Environ.* **2021**, *752*, 141854. [[CrossRef](#)]
41. Chin, J.F.; Heng, Z.W.; Teoh, H.C.; Chong, W.C.; Pang, Y.L. Recent development of magnetic biochar crosslinked chitosan on heavy metal removal from wastewater—Modification, application and mechanism. *Chemosphere* **2022**, *291*, 133035. [[CrossRef](#)]

42. Mo, H.; Qiu, J. Preparation of Chitosan/Magnetic Porous Biochar as Support for Cellulase Immobilization by Using Glutaraldehyde. *Polymers* **2020**, *12*, 2672. [[CrossRef](#)]
43. Han, R.; Li, W.; Pan, W.; Zhu, M.; Zhou, D.; Li, F.S. 1D Magnetic Materials of Fe₃O₄ and Fe with High Performance of Microwave Absorption Fabricated by Electrospinning Method. *Sci. Rep.* **2014**, *4*, 7493. [[CrossRef](#)]
44. Mo, H.; Qiu, J.; Yang, C.; Zang, L.; Sakai, E.; Chen, J. Porous biochar/chitosan composites for high performance cellulase immobilization by glutaraldehyde. *Enzym. Microb. Technol.* **2020**, *138*, 109561. [[CrossRef](#)] [[PubMed](#)]
45. Zhou, X.; Zhou, J.; Liu, Y.; Guo, J.; Ren, J.; Zhou, F. Preparation of iminodiacetic acid-modified magnetic biochar by carbonization, magnetization and functional modification for Cd(II) removal in water. *Fuel* **2018**, *233*, 469–479. [[CrossRef](#)]
46. Wang, F.; Li, L.; Iqbal, J.; Yang, Z.; Du, Y. Preparation of magnetic chitosan corn straw biochar and its application in adsorption of amaranth dye in aqueous solution. *J. Biol. Macromol.* **2022**, *199*, 234–242. [[CrossRef](#)] [[PubMed](#)]
47. Zhao, Y.; Zhang, R.; Liu, H.; Li, M.; Chen, T.; Chen, D.; Zou, X.; Frost, R.L. Green preparation of magnetic biochar for the effective accumulation of Pb(II): Performance and mechanism. *Chem. Eng. J.* **2019**, *375*, 122011. [[CrossRef](#)]
48. Baghban, N.; Yilmaz, E.; Soylak, M. A magnetic MoS₂-Fe₃O₄ nanocomposite as an effective adsorbent for dispersive solid-phase microextraction of lead(II) and copper(II) prior to their determination by FAAS. *Microchim. Acta* **2017**, *184*, 3969–3976. [[CrossRef](#)]
49. Vigneshwaran, S.; Sirajudheen, P.; Nikitha, M.; Ramkumar, K.; Meenakshi, S. Facile synthesis of sulfur-doped chitosan/biochar derived from tapioca peel for the removal of organic dyes: Isotherm, kinetics and mechanisms. *J. Mol. Liq.* **2021**, *326*, 115303. [[CrossRef](#)]
50. Palansooriya, K.N.; Kim, S.; Igalavithana, A.D.; Hashimoto, Y.; Choi, Y.-E.; Mukhopadhyay, R.; Sarkar, B.; Ok, Y.S. Fe(III) loaded chitosan-biochar composite fibers for the removal of phosphate from water. *J. Hazard. Mater.* **2021**, *415*, 125464. [[CrossRef](#)]
51. Zhang, P.; Zhang, N.; Wang, Q.; Wang, P.; Yuan, J.; Shen, J.; Fan, X. Disulfide bond reconstruction: A novel approach for grafting of thiolated chitosan onto wool. *Carbohydr. Polym.* **2019**, *203*, 369–377. [[CrossRef](#)]
52. Teng, D.; Zhang, B.; Xu, G.; Wang, B.; Mao, K.; Wang, J.; Sun, J.; Feng, X.; Yang, Z.; Zhang, H. Efficient removal of Cd(II) from aqueous solution by pinecone biochar: Sorption performance and governing mechanisms. *Environ. Pollut.* **2020**, *265* (Pt A), 115001. [[CrossRef](#)]
53. Song, J.; Messele, S.A.; Meng, L.; Huang, Z.; Gamal El-Din, M. Adsorption of metals from oil sands process water (OSPW) under natural pH by sludge-based Biochar/Chitosan composite. *Water Res.* **2021**, *194*, 116930. [[CrossRef](#)]
54. Yamashita, T.; Hayes, P. Analysis of XPS spectra of Fe²⁺ and Fe³⁺ ions in oxide materials. *Appl. Surf. Sci.* **2008**, *254*, 2441–2449. [[CrossRef](#)]
55. Ji, J.; Chen, G.; Zhao, J. Preparation and characterization of amino/thiol bifunctionalized magnetic nanoadsorbent and its application in rapid removal of Pb (II) from aqueous system. *J. Hazard. Mater.* **2019**, *368*, 255–263. [[CrossRef](#)]
56. Ma, Y.X.; Xing, D.; Shao, W.J.; Du, X.Y.; La, P.Q. Preparation of polyamidoamine dendrimers functionalized magnetic graphene oxide for the adsorption of Hg(II) in aqueous solution. *J. Colloid Interface Sci.* **2017**, *505*, 352–363. [[CrossRef](#)]
57. Shahrin, E.W.E.; Narudin, N.A.H.; Shahri, N.N.M.; Nur, M.; Lim, J.-W.; Bilad, M.R.; Mahadi, A.H.; Hobley, J.; Usman, A. A comparative study of adsorption behavior of rifampicin, streptomycin, and ibuprofen contaminants from aqueous solutions onto chitosan: Dynamic interactions, kinetics, diffusions, and mechanisms. *Emerg. Contam.* **2022**, *9*, 100199. [[CrossRef](#)]
58. Fang, W.; Jiang, X.; Luo, H.; Geng, J. Synthesis of graphene/SiO₂@polypyrrole nanocomposites and their application for Cr(VI) removal in aqueous solution. *Chemosphere* **2018**, *197*, 594–602. [[CrossRef](#)]
59. Kim, S.A.; Kamala-Kannan, S.; Lee, K.-J.; Park, Y.-J.; Shea, P.J.; Lee, W.-H.; Kim, H.-M.; Oh, B.-T. Removal of Pb(II) from aqueous solution by a zeolite-nanoscale zero-valent iron composite. *Chem. Eng. J.* **2013**, *217*, 54–60. [[CrossRef](#)]
60. Wang, H.; Yuan, X.; Wu, Y.; Chen, X.; Leng, L.; Wang, H.; Li, H.; Zeng, G. Facile synthesis of polypyrrole decorated reduced graphene oxide-Fe₃O₄ magnetic composites and its application for the Cr(VI) removal. *Chem. Eng. J.* **2015**, *262*, 597–606. [[CrossRef](#)]
61. Xiang, L.; Niu, C.-G.; Tang, N.; Lv, X.-X.; Guo, H.; Li, Z.-W.; Liu, H.-Y.; Lin, L.-S.; Yang, Y.-Y.; Liang, C. Polypyrrole coated molybdenum disulfide composites as adsorbent for enhanced removal of Cr(VI) in aqueous solutions by adsorption combined with reduction. *Chem. Eng. J.* **2021**, *408*, 127281. [[CrossRef](#)]
62. Yi, Y.; Tu, G.; Zhao, D.; Tsang, P.E.; Fang, Z. Key role of FeO in the reduction of Cr(VI) by magnetic biochar synthesised using steel pickling waste liquor and sugarcane bagasse. *J. Clean. Prod.* **2020**, *245*, 118886. [[CrossRef](#)]
63. Ko, D.; Lee, J.S.; Patel, H.A.; Jakobsen, M.H.; Hwang, Y.; Yavuz, C.T.; Hansen, H.C.B.; Andersen, H.R. Selective removal of heavy metal ions by disulfide linked polymer networks. *J. Hazard. Mater.* **2017**, *332*, 140–148. [[CrossRef](#)]
64. Zhu, K.; Gao, Y.; Tan, X.; Chen, C. Polyaniline-Modified Mg/Al Layered Double Hydroxide Composites and Their Application in Efficient Removal of Cr(VI). *ACS Sustain. Chem. Eng.* **2016**, *4*, 4361–4369. [[CrossRef](#)]
65. Prajapati, A.K.; Das, S.; Mondal, M.K. Exhaustive studies on toxic Cr(VI) removal mechanism from aqueous solution using activated carbon of Aloe vera waste leaves. *J. Mol. Liq.* **2020**, *307*, 112956. [[CrossRef](#)]
66. Zhang, S.L.; Wang, Z.K.; Chen, H.Y.; Kai, C.C.; Jiang, M.; Wang, Q.; Zhou, Z.W. Polyethylenimine functionalized Fe₃O₄/steam-exploded rice straw composite as an efficient adsorbent for Cr(VI) removal. *Appl. Surf. Sci.* **2018**, *440*, 1277–1285. [[CrossRef](#)]
67. Lin, C.; Luo, W.J.; Luo, T.T.; Zhou, Q.; Li, H.F.; Jing, L.R. A study on adsorption of Cr (VI) by modified rice straw: Characteristics, performances and mechanism. *J. Clean. Prod.* **2018**, *196*, 626–634. [[CrossRef](#)]

68. Chen, S.; Yue, Q.; Gao, B.; Li, Q.; Xu, X. Removal of Cr(Vi) from Aqueous Solution Using Modified Corn Stalks: Characteristic, Equilibrium, Kinetic and Thermodynamic Study. *Chem. Eng. J.* **2011**, *168*, 909–917. [[CrossRef](#)]
69. Zhao, N.; Yin, Z.; Liu, F.; Zhang, M.; Lv, Y.; Hao, Z.; Pan, G.; Zhang, J. Environmentally persistent free radicals mediated removal of Cr(VI) from highly saline water by corn straw biochars. *Bioresour. Technol.* **2018**, *260*, 294–301. [[CrossRef](#)] [[PubMed](#)]

Disclaimer/Publisher's Note: The statements, opinions and data contained in all publications are solely those of the individual author(s) and contributor(s) and not of MDPI and/or the editor(s). MDPI and/or the editor(s) disclaim responsibility for any injury to people or property resulting from any ideas, methods, instructions or products referred to in the content.